Article

Facile Redox Synthesis of Novel Bimetallic Cr^{n+}/Pd^0 Nanoparticles Supported on SiO_2 and TiO_2 for Catalytic Selective Hydrogenation with Molecular Hydrogen

Olga A. Kirichenko [1,2,*], Elena A. Redina [1,*] , Gennady I. Kapustin [1], Marina S. Chernova [1], Anastasiya A. Shesterkina [1,3] and Leonid M. Kustov [1,4]

[1] N.D. Zelinsky Institute of Organic Chemistry, Russian Academy of Sciences, 47 Leninsky Prospect, 119991 Moscow, Russia; gik@ioc.ac.ru (G.I.K.); marina.chernova.1998@inbox.ru (M.S.C.); anastasiia.strelkova@mail.ru (A.A.S.); lmk@ioc.ac.ru (L.M.K.)

[2] M.V. Lomonosov Institute of Fine Chemical Technologies, Russian Technological University MIREA, 86 Vernadsky Prospect, 119571 Moscow, Russia

[3] Nanochemistry and Ecology Department, National University of Science and Technology (MISiS), 2 Leninsky Prospect, 119991 Moscow, Russia

[4] Chemistry Department, Moscow State University, Leninskie Gory 1, Bldg. 3, 119992 Moscow, Russia

[*] Correspondence: okiriche@hotmail.com or okiriche@ioc.ac.ru (O.A.K.); redinaea@ioc.ac.ru (E.A.R.)

Abstract: The bimetallic Cr^{n+}/Pd^0 nanoparticles have been synthesized for the first time by a two-step redox method. The method includes the deposition of Pd^0 nanoparticles on the surface of SiO_2 and TiO_2 carriers followed by the deposition of Cr^{n+} on the surface of Pd^0 nanoparticles using the redox procedures, which are based on the catalytic reduction of Cr^{n+} with H_2 in aqueous suspensions at ambient conditions. Transmission (TEM) and scanning (SEM) electron microscopy, X-ray photoelectron spectroscopy (XPS), Fourie-transformed infrared spectroscopy of adsorbed CO (FTIR-CO), and CO chemisorption studies were performed to characterize the morphology, nanoparticle size, element, and particle distribution, as well as the electronic state of deposited metals in the obtained catalysts. A decrease in nanoparticle size from 22 nm (Pd/SiO_2) to 2–6 nm (Pd/TiO_2) makes possible deposition of up to 1.1 wt.% Cr most likely as Cr^{3+}. The deposition of CrO_x species on the surface of Pd nanoparticles was confirmed using FTIR of adsorbed CO and the method of temperature-programmed reduction with hydrogen ($TPR-H_2$). The intensive hydrogen consumption in the temperature ranges from -50 °C to 40 °C ($Cr/Pd/SiO_2$) and from -90 °C to -40 °C ($Cr/Pd/TiO_2$) was first observed for the supported Pd catalysts. The decrease in the temperature of β-PdH_x decomposition indicates the strong interaction between the deposited Cr^{n+} species and Pd^0 nanoparticle after reduction with H_2 at 500 °C. The novel $Cr^{n+}/Pd/TiO_2$ catalysts demonstrated a considerably higher activity in selective hydrogenation of phenylacetylene than the Pd/TiO_2 catalyst at ambient conditions.

Keywords: CrO_x/Pd nanoparticles; bimetallic nanoparticle preparation; $TPR-H_2$; selective hydrogenation

1. Introduction

Palladium has unique properties in the catalysis of diverse reactions [1–5]. Modification of Pd nanoparticles in the catalytic materials is currently considered as a promising way to improve the catalytic properties of Pd-based materials, especially in selective hydrogenation of organic compounds [6–9]. The promotion of Pd with Ga, Zn, In, Pb, Cu, Bi, Te, Ce, Zr [7,8,10,11], Sn, Ni, Pb, Ag, Au, Pt, Rh, Ru, Cu, Co, Ge, [9], Fe [12–16] has been successfully used. There is no single interpretation to explain the effect of second metal on the performance of Pd catalysts. Depending on the nature of both the co-metal and the reaction, the beneficial presence of a co-metal was interpreted in terms of geometric effects, electronic effects, and mixed sites. In the case of partly reduced second metal Pd–M^{n+},

the promoting effect was attributed to a positively charged cationic species M^{n+} activating the functional groups of a substrate, which becomes easily hydrogenated. Electronic modifications upon alloying Pd were used to interpret the better selectivity observed in the selective hydrogenation of alkadienes and alkynes to alkenes. The presence of the second metal at the surface or in the bulk was shown to change the relative adsorption strength of the alkynes, alkadienes, and alkenes, which resulted in an increased reactivity for alkynes and a decreased reactivity for alkenes.

The influence of Cr additives on the catalytic behavior of Pd catalysts in selective hydrogenation is poorly studied, and contradictory results were obtained for Cr-Pd catalysts. When chromium is incorporated in the network of palladium in the charcoal supported Pd-Cr catalysts, the catalysts became more active in the hydrogenation of 1,3-butadiene and fully selective for the formation of butenes [17]. Introduction of both Cr^{6+} by impregnation with an aqueous solution of Pd-Cr mixed salts and Cr^0 by vapor deposition onto the Pd/SiO_2 catalysts was shown to decrease the activity in hydrogenation of double C=C bonds thus improving the selectivity in the partial hydrogenation of butadiene [18]. In these catalysts, Pd^0 facilitates the reduction of CrO_x nanoparticles to Cr^0 at 600 °C. The Cr deposition using impregnation with ammonium chromate followed by calcination at 550 °C strongly enhanced the sulfur resistance of supported Pd-based catalysts, as well as the activity in toluene hydrogenation that increased with the Cr/Pd atomic ratio and reached its maximum when the Cr/Pd was equal to 8 [19]. Methylcyclohexane and dimethylcyclopentane were the main products. Recent studies revealed that the deposition-precipitation of Pd^0 nanoparticles on TiO_2 support in the presence of CrO_4^{2-} ions resulted in changes of the redox behavior of the materials and improving the catalytic properties in dehydrogenation and hydrogenation of aromatics [20].

The goal of the present work is to reveal the conditions of redox-deposition of CrO_x species from H_2CrO_4 aqua solution on the surface of supported Pd nanoparticles, their further reduction with H_2, as well as to evaluate the influence of thus deposited CrO_x species on the catalytic activity of Pd catalysts in hydrogenation of unsaturated bonds on an example of phenylacetylene (PhA) hydrogenation. Two catalysts consisting from Pd nanoparticles on a support were selected as initial samples: (i) $3\%Pd/SiO_2$, whose redox-modifying with iron oxide resulted in enhanced PhA selective hydrogenation [21]; it was taken as a reference sample; (ii) $1\%Pd/TiO_2$, whose redox-modifying with chromium oxide resulted in improving the catalytic properties in dehydrogenation and hydrogenation of aromatics [20]. It should be also mentioned, that hexavalent chromium (Cr^{6+}) possesses high toxicity [22]. However, chromium acid is actively used in many industries, in which a large amount of waste chromic acid solution is generated [23]. The involvement of such waste chromic acid in the production of a new type of Cr-Pd catalytic systems, where CrO_4^{2-} ions are reduced to nontoxic Cr_2O_3 or $Cr(OH)_3$ species, seems to be an attractive way of waste chromic acid utilization.

2. Results and Discussion

The preparation methods of bimetallic Pd catalysts influence the chemical state and the spatial distribution of both components thus affecting the catalytic behavior [8]. To control the Cr^{n+} effect, the modifier should be deposited on the Pd nanoparticle surface in a proper way, and low reaction temperatures are preferable to avoid the formation of alloys. The deposition of a second metal on the surface of a noble metal as a three-dimensional deposit is possible by the method of a redox reaction with adsorbed species (RRA) [24]. A reductant that is preadsorbed selectively on the primary metal reduces the ions of the second metal, causing its deposition on the surface of primary metals, and two metals interact. Hydrogen, which is pre-adsorbed on the noble metals, is commonly used to prepare bimetallic catalysts by RRA. For instance, by using pre-adsorbed hydrogen and RRA, Pt [25] and Au [26] were deposited on reduced Pd^0 particles. Recently it was shown that a transition metal oxide (iron oxide) can be deposited on the Pd nanoparticle surface by the modified RRA techniques that supposed the primary RRA deposition of a water-
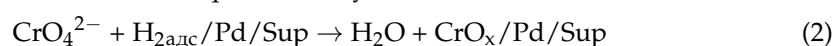
insoluble inorganic salt of transition metal [21]. Here we propose the redox method based on the following facts. The Pd-adsorbed H_2 is shown [20] can be effective for supporting the metal oxide species onto the surface of precious metal nanoparticles via reduction of a soluble anion, which contained a transition metal in the highest oxidation state, to the insoluble hydroxide of metal in the lower oxidation state. The direct redox reaction between CrO_4^{2-} and H_2 is impossible in an aqueous solution at room temperature. The adsorption of CrO_4^{2-} anions on the SiO_2 and TiO_2 surface cannot proceed at pH higher than the point of zero charge varying in the range 1–4.2 for the different silica materials and equal to 6.3 for the commercial TiO_2 Degussa P-25 [27]. Therefore, it is conceivable to perform RRA precipitation only on the surface of Pd nanoparticles maintaining a high enough pH value. Strategies for the CrO_x deposition on the surface of Pd nanoparticles via the RRA method can be presented as following schemes ("Sup" means support):

1. Reduction by preadsorbed hydrogen (RA procedure):

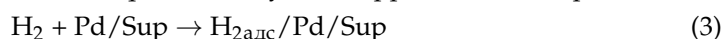- Preliminary H_2 adsorption from a gas flow on a supported Pd nanoparticle

$$H_2 + Pd/Sup \rightarrow H_{2адс}/Pd/Sup \tag{1}$$
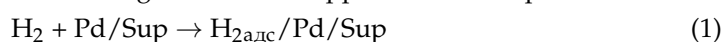
- Subsequent redox reaction in aqueous slurry

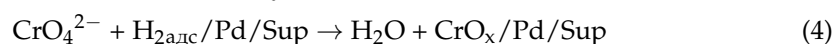$$CrO_4^{2-} + H_{2адс}/Pd/Sup \rightarrow H_2O + CrO_x/Pd/Sup \tag{2}$$

2. Catalytic reduction by gaseous hydrogen (RC procedure):

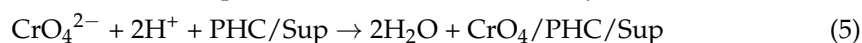- Permanent H_2 adsorption in an aqueous slurry on a supported Pd nanoparticle

$$H_2 + Pd/Sup \rightarrow H_{2адс}/Pd/Sup \tag{3}$$

- Simultaneous redox reaction in slurry

$$CrO_4^{2-} + H_{2адс}/Pd/Sup \rightarrow H_2O + CrO_x/Pd/Sup \tag{4}$$

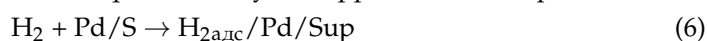3. Co-reduction with the supported polyhydroxo complexes (PHC) of Pd (CoR procedure):

- Preliminary CrO_4^{2-} chemisorption from solution in the slurry
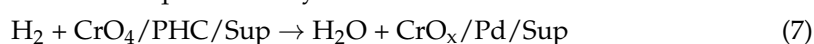
$$CrO_4^{2-} + 2H^+ + PHC/Sup \rightarrow 2H_2O + CrO_4/PHC/Sup \tag{5}$$

- Permanent H_2 adsorption in an aqueous slurry on supported Pd nanoparticle

$$H_2 + Pd/S \rightarrow H_{2адс}/Pd/Sup \tag{6}$$

- Simultaneous reduction in aqueous slurry

$$H_2 + CrO_4/PHC/Sup \rightarrow H_2O + CrO_x/Pd/Sup \tag{7}$$

$$H_2 + PHC/Sup \rightarrow H_2O + Pd/Sup \tag{8}$$

$$CrO_4^{2-} + H_{2адс}/Pd/Sup \rightarrow H_2O + CrO_x/Pd/Sup \tag{9}$$
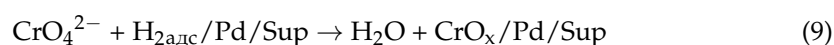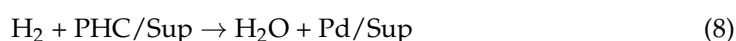
2.1. Elemental Composition, Nanoparticle Size and Morphology

The deposited amount of Cr^{n+} for the samples on 3%Pd/SiO$_2$ (Pd/S) was found to be limited both for the RA and RC procedures and was slightly larger for the RC procedure. According to calculations based on Cr concentration in solutions, Cr loading in the sample was supposed to be 0.50 wt.%, but it was only 0.26 wt.% for Cr/Pd/S-RA and 0.36 wt.% for Cr/Pd/S-RC samples because of incomplete Cr^{6+} removal from solutions.

For 1%Pd/TiO$_2$ (Pd/T) sample and its precursor PHC/TiO$_2$, complete removal of Cr^{6+} from solutions were obtained at the conditions presented in Table 1, and the higher Cr loading values have been reached by both RC and CoR procedures. The possibility of wider variation in Cr loading opened the prospects for studies; therefore, more intensive characterization of the Cr/Pd/T samples has been done.

The electron microscopy studies of the obtained samples showed the influence of the preparation method on the morphology, the particle size distribution, and the element spreading over the sample. On the SEM images of selected samples, one can see the secondary structures consisted of the agglomerates of round-shaped particles (Figures 1 and S1).

Table 1. Catalyst composition and conditions of synthesis.

Sample	Cr, wt.%	Cr:Pd$_v$	[Cr^{6+}], mmol L^{-1}	τ_{RR}, h	pH$_i$	pH$_{ms}$
Cr/Pd/S-RA	0.026	0.018	2.6	2	-	-
Cr/Pd/S-RA	0.260	0.180	26.0	18	4.4	-
Cr/Pd/S-RC	0.360	0.740	1.5	25	4.4	8.3
Cr/Pd/T-RC	0.360	0.740	5.9	5	2.8	8.3
Cr/Pd/T-RC-2	0.720	1.50	12.0	3	2.7	10.3
Cr/Pd/T-RC-3	1.10	2.20	18.0	3	2.6	10.7
Cr/Pd/T-CoR	0.360	0.740	2.9	6	5.7	9.7
Cr/Pd/T-CoR-2	0.430	0.870	3.5	6	5.3	9.5

Cr:Pd$_v$—the element atomic ratio in a sample; [Cr^{6+}]—initial Cr concentration in a solution of a slurry; τ_{RR}—time of redox reaction in a slurry; pH$_i$ and pH$_{ms}$—pH of solutions before and after reduction in a slurry. S—SiO$_2$ support, T—TiO$_2$ support. RA—reduction by preadsorbed hydrogen; RC—catalytic reduction by gaseous hydrogen; CoR—co-reduction with the supported polyhydroxo complexes of Pd (PHC).
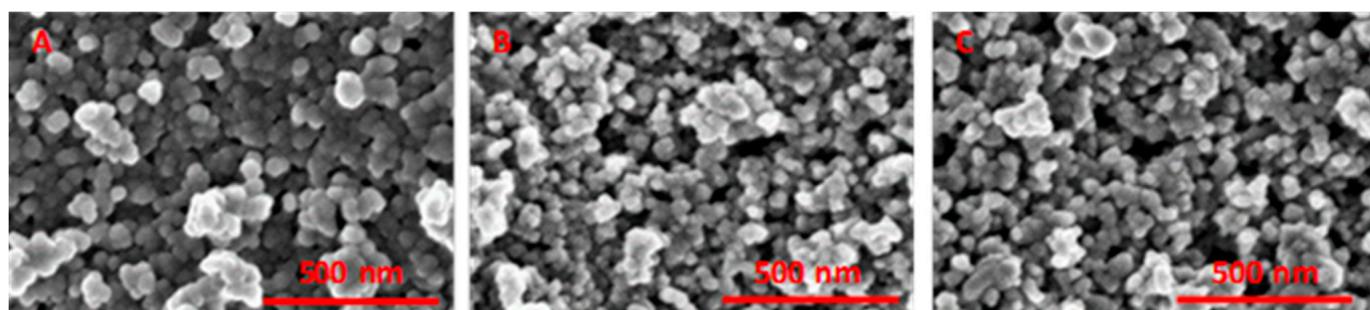
Figure 1. SEM images of the samples: (**A**) Cr/Pd/T-CoR; (**B**) Cr/Pd/T-RC; (**C**) Cr/Pd/T-RC-3.

According to SEM-EDX analysis data, in all samples, Cr was uniformly distributed throughout the sample with random areas of increased concentration. The local areas of high and low concentration of Pd were also observed, especially in the sample Cr/Pd/T-CoR (Figure 2A). It seems that during the CoR preparation a weakly acidic environment is created in the Pd-PHC/TiO$_2$ suspension after the addition of a chromic acid solution which leads to the partial dissolution of PHC (especially, at 60 °C) and the transfer of palladium ions into the solution. Further, two main processes are possible: (1) transfer of Pd ions in the solution, leading to the growth of PHC particles and their aggregates and resulting in the appearance of local regions with high and low Pd concentrations at a normal total Pd content; (2) adsorption of Pd cations on the support surface followed by their reduction and the surface diffusion of Pd atoms with the formation of clusters that serve as the new centers of redox deposition of Cr particles, and the result is a uniform Cr distribution. The deposition of Cr species via RC-method, i.e., after supporting and reduction of Pd-PHC to metallic Pd^0 nanoparticles, resulted in more uniform Pd and Cr distribution in the sample with the same Pd loading (Figure 2B). It is most likely due to the weak dissolution of metallic Pd and the less possible effect of Pd redispersion on the surface of TiO$_2$. However, the areas with the increased local concentration of both Pd and Cr appeared with further increase of Cr loading in the samples prepared by RC procedure (Figure 2C), and the slightly stronger acidity of the initial solution might be a reason for this redistribution (Table 1).
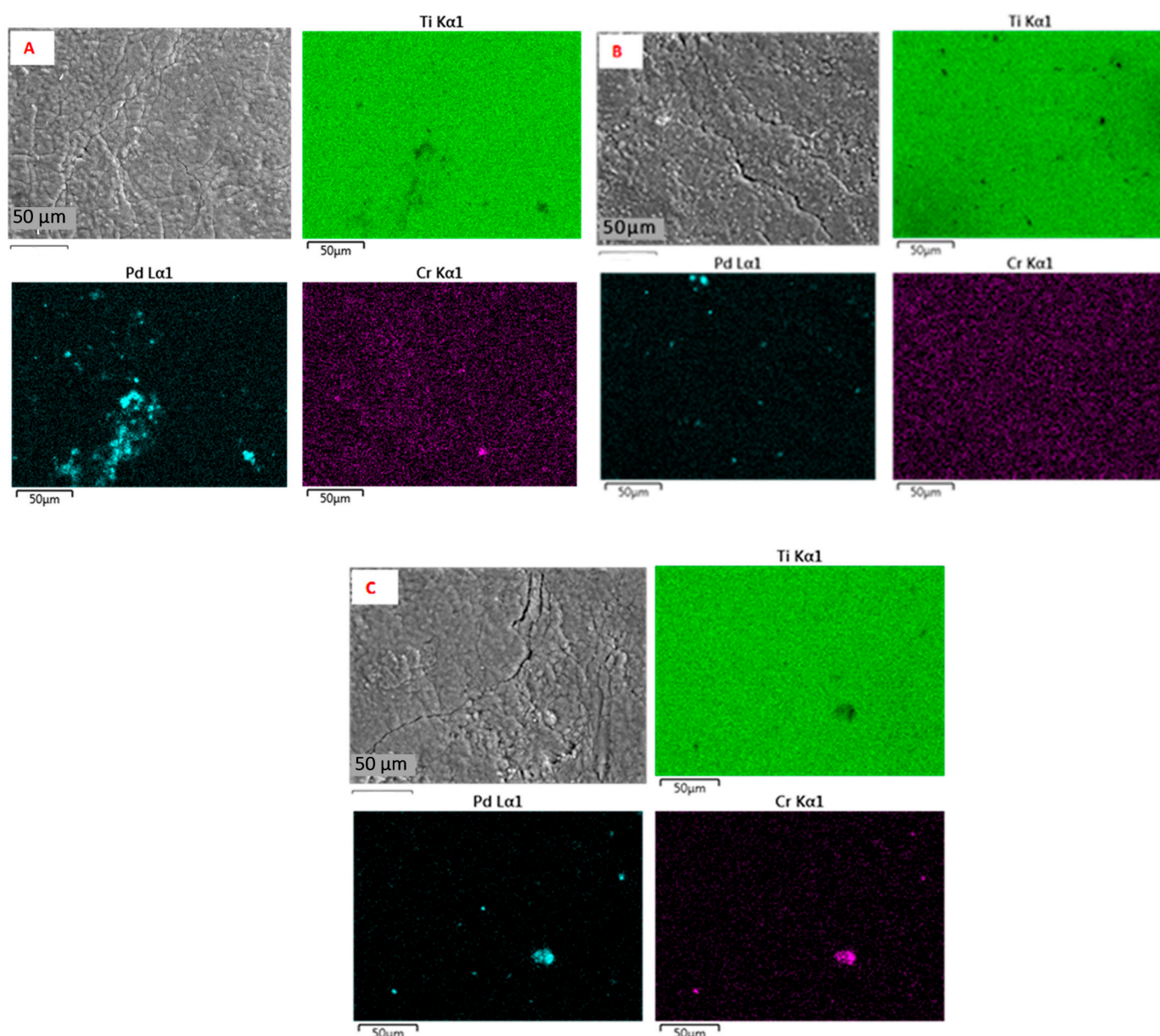
Figure 2. SEM-EDX maps for the samples: (**A**) Cr/Pd/T-CoR; (**B**) Cr/Pd/T-RC; (**C**) Cr/Pd/T-RC-3.

The TEM study (Figure 3, Figure S2) revealed a narrow particle size distribution with a mean particle size of 3.7 nm for the Cr/Pd/T-CoR sample, while the sample of the same composition prepared by the RC method is characterized by the shift of particle size distribution to the higher values with a mean particle size of 4.1 nm. Therefore, the assumption of surface diffusion of palladium atoms with the formation of clusters that serve as new centers of redox deposition of chromium particles during the CoR method is more plausible. Redispersion of Pd in acidic slurry seems to occur also during the RC method under deposition of a higher amount of Cr species from more concentrated chromium acid, and smaller particles are observed in Cr/Pd/T-RC-3 sample than in the catalyst Cr/Pd/T-RC.
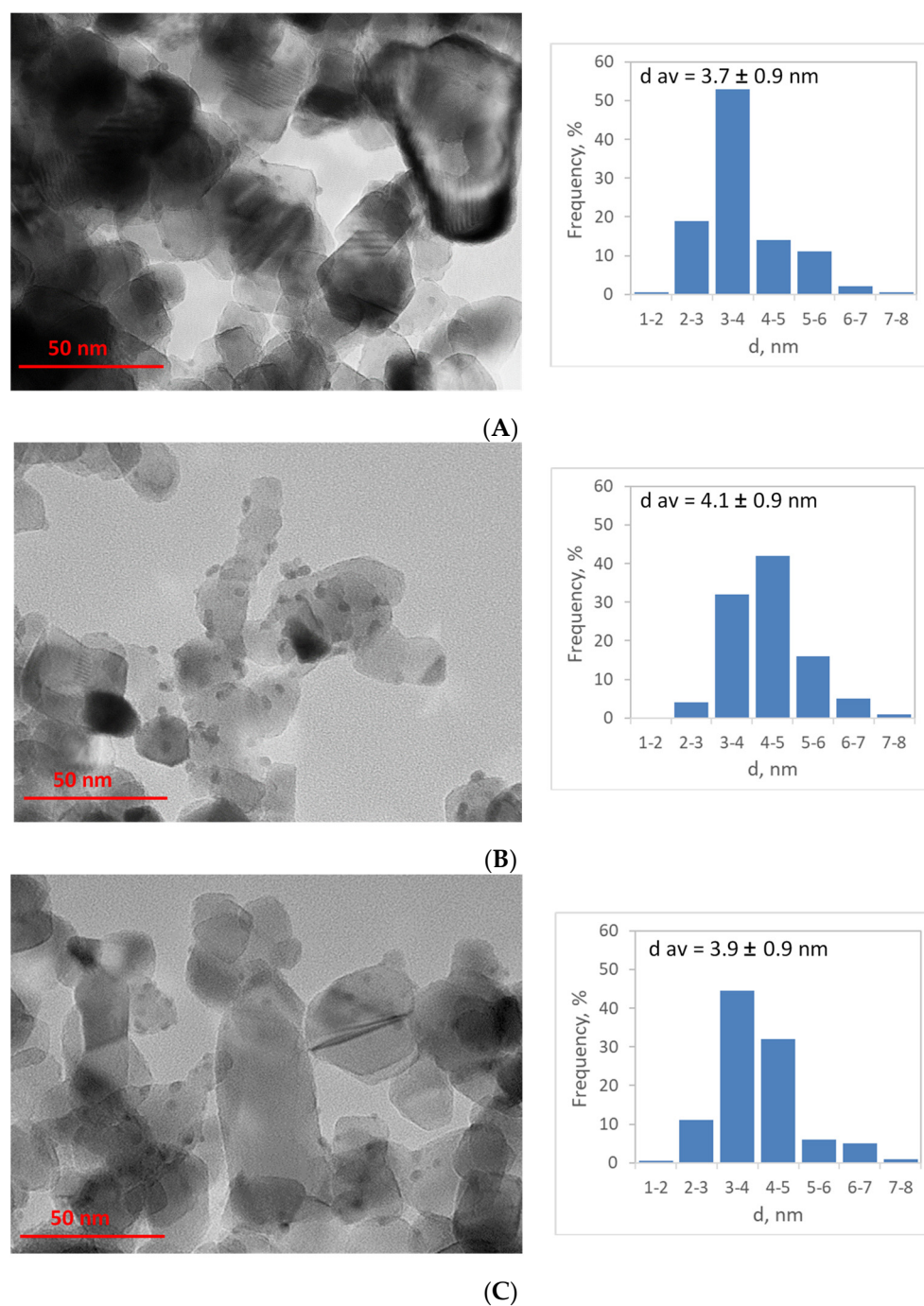
Figure 3. TEM images and particle size distribution of the samples: (**A**) Cr/Pd/T-CoR; (**B**) Cr/Pd/T-RC; (**C**) Cr/Pd/T-RC-3.

The XPS survey spectra show that the surface of samples is composed mainly of oxygen, titanium, carbon, palladium. The Cr peaks have been reliably recorded in the survey spectrum only for the sample Cr/Pd/T-RC-3 with the highest Cr loading of 1.1 wt.% (Figure 4a). Overlapping of Cr 2p region with Ti 2s region hindered revealing the lower Cr loadings. No peaks Cl $2p_{3/2}$ were found at 198.8 eV or 198.2 eV, which exhibits the absence of chloride ion in the palladium environment [28] and Ti-Cl bonds [29], suggesting good washing of the samples during their preparations.

Figure 4. The XPS spectra for the sample Cr/Pd/T-RC-3: (**a**) the survey spectrum (**b**) high-resolution spectrum and curve fits to the Pd 3d region; (**c**) high-resolution Cr 2p spectrum.

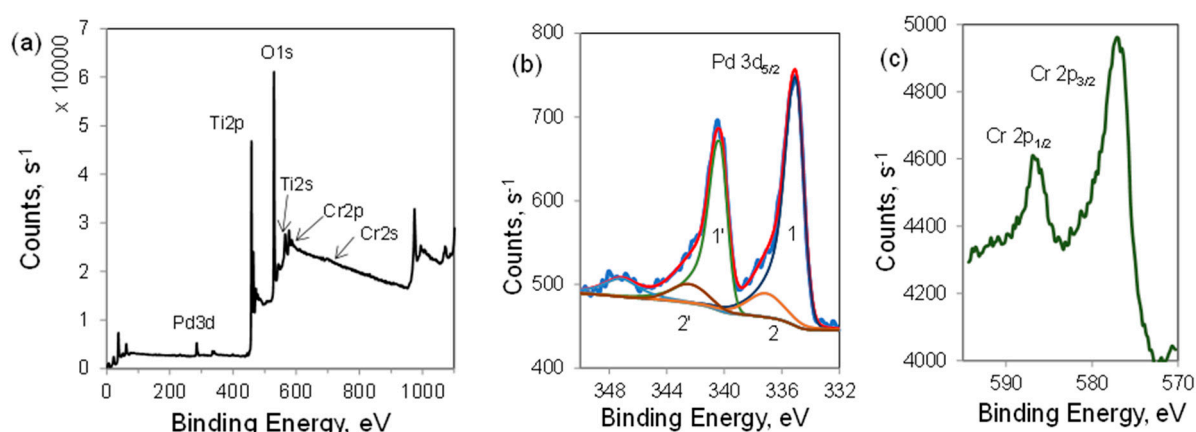Analysis of the wide-scan XPS spectra of the surface for the samples Cr/Pd/T prepared by RC and CoR procedure shows no significant difference in the atomic percentages of the elements (Table 2). The presence of carbon and increased O/Ti atomic ratio is the feature of commercial TiO_2 aerooxide P-25. The obtained atomic ratios O/Ti and C/Ti (Table 2) are similar to those found previously for P-25 produced by Germanic Degussa Co (Frankfurt, Germany) [27].

Table 2. The element atomic percentages (at. %) and their relative concentrations on the surface.

Sample	O 1s	Ti 2p	C 1s	Pd 3d	Cr 2p1/2	O/Ti	C/Ti
Cr/Pd/T-CoR	60.5	23.5	14.5	0.6	-	2.6	0.6
Cr/Pd/T-RC	60.4	23.4	15.4	0.6	-	2.6	0.7
Cr/Pd/T-RC-3	61.0	23.1	13.0	0.5	1.4	2.6	0.6

RC—catalytic reduction by gaseous hydrogen; CoR—co-reduction with the supported polyhydroxo complexes of Pd (PHC).

XPS analysis has revealed Pd enrichment over the TiO_2 surface to 2.2 wt.%, as compared with a bulk Pd loading of 1.0 wt.%, which can be due to the deposition of small Pd nanoparticles of the size of 2–6 nm on the surface of nonporous TiO_2 particles with considerably larger size of more than 20 nm. The atomic ratio Cr:Pd was 2.8 that is considerably higher than the value calculated for the bulk chemical composition of the sample Cr/Pd/T-RC-3 (Table 1). The calculated surface Cr concentration of 3.1 wt.% exceeds the Cr loading in the sample, which indicates high dispersion of the deposited Cr species.

The high-resolution spectra of Ti 2p are identical for all samples and correlate to TiO_2. Figure 4b represents the high-resolution spectrum of the Pd 3d region recorded for the Cr/Pd/T-RC-3 sample. As shown in Figure 4b, the Pd state can be reproduced as a sum of two doublets $3d_{5/2}$ and $3d_{3/2}$: 1-1′ main peaks and one satellite (asymmetry like in metallic Pd^0) and 2-2′ symmetric peaks corresponding to Pd^{n+}. The most important spectral parameter values obtained as a result of the fitting are presented in Table 3. The obtained BE (binding energy) values for Pd^{n+} are between reported for PdO 336.3 eV and for PdO_2 [30], and Pd^{n+} content is low. The variations in the calculated values are within the experimental errors (BE $\pm$ 0.2 eV, HW $\pm$ 0.02 eV, I $\pm$ 5%) excepting electrostatic charge that is lower in the samples prepared by RC procedure, which allowed us to conclude that neither the preparation procedure nor Cr loading affected Pd electronic state.

Table 3. Results of the Pd 3d spectra approximation for Cr/Pd/TiO$_2$ samples.

Catalyst	Spectral Parameters	Pd 3d		
		1-1′ Pd^0	2-2′ Pd^{2+}	Satellite Pd^0
	BE, eV	335.1	337.1	347.4
Cr/Pd/T-CoR	Half width, eV	1.3	3.0	3.0
	Intensity, %	76	14	10
	BE, eV	335.1	337.2	347.2
Cr/Pd/T-RC-2	Half width, eV	1.3	3.0	3.0
	Intensity, %	77	16	7
	BE, eV	335.1	337.2	347.2
Cr/Pd/T-RC-3	Half width, eV	1.3	3.0	3.0
	Intensity, %	79	14	7

RC—catalytic reduction by gaseous hydrogen; CoR—co-reduction with the supported polyhydroxo complexes of Pd (PHC).

The spectrum of the Cr 2p region was clearly observed only for the sample with the highest Cr content of 1.1 wt.% (Figure 4c). Its shape is distorted due to overlapping with Ti 2s, nevertheless, BE can be estimated as 576.9–577.4 eV that can be assigned to Cr^{3+} in Cr$_2$O$_3$ (576,5 eV) [31,32] and in surface species CrO$_x$ (577.0–577.6 eV) [33] or more likely in Cr(OH)$_3$ (577.3 eV) [34,35]. It should be pointed out that Cr(OH)$_3$ is the major Cr component of passive layers electrochemically formed on alloys in aqueous solutions. It seems that Cr^{6+} content is very small. Would chromium be present in the two main oxidation states: Cr^{3+} and Cr^{6+} in comparable amounts (at least 21.3 relative %), the doublet should be observed in the spectrum due to the chemical shift (binding energy separation) between the Cr^{3+} and Cr^{6+} [31]. However, light asymmetry of Cr2p peak at 578–583 eV suppose that presence of smaller portions of Cr^{6+} cannot be excluded. BE of Cr^{6+} in 13%Cr$_2$O$_3$/Al$_2$O$_3$ sample, which was partly oxidized at 600 °C, was found to be 579.3 eV [29]. For Cr/ZrO$_2$ samples after redox cycles BE of Cr^{6+} varied 578.8–579.5 eV [36].

Figure 5 shows FTIR spectra of CO adsorbed on the Pd/T and Cr/Pd/T samples. The IR spectra of CO absorbed on Pd can be divided into two regions: linear CO (2000–2100 cm^{-1}) and multi-coordinated (two or three-coordinated) CO (1995–1800 cm^{-1}). The part of the spectra due to linearly adsorbed CO is represented by a sharp band about 2085–2090 cm^{-1} due to CO residing on corner Pd atoms with a low-frequency shoulder at about 2050 cm^{-1} due to, most probably, CO bound to (111/111) and (111/100) particle edges [37]. The intensity of these bands slightly increased for the sample Cr/Pd/T-CoR which can be due to the decrease in the particle size that was observed with TEM (Figure 3). The opposite changes were observed after Cr deposition on the Pd nanoparticles surface by RC method at the same Cr loading, which may be due to the partial blocking of the Pd sites on the corner Pd atoms and the Pd particle edges with CrO$_x$ species. For all samples, the part of the spectra related to multi coordinated CO contains a band at 1980 cm^{-1} that can be assigned to two-coordinated (bridged) CO on Pd(100) facets [37]. The significantly decreased intensity of this band in the spectrum of the sample Cr/Pd/T-RC indicates the possible redox deposition of CrO$_x$ species on Pd(100) facets. In addition, the spectrum of CO adsorbed on the Pd/T sample contains a broad band at 1920 cm^{-1} while the spectra of CO on Cr/Pd/T-CoR and Cr/Pd/T-RC samples contain an intense broad band at about 1900 cm^{-1}. The band at 1920 cm^{-1} is due to either bridged CO on particle edges or three-coordinated CO on Pd(111) facets [37,38]. The band at about 1900 cm^{-1} can be assigned to three-coordinated CO on Pd(111) or bridged CO on (100) planes. The tailing of the spectra below 1850 cm^{-1} can be explained by the presence of additional broad and poorly-resolved absorption bands around 1800 cm^{-1}. The absorption around 1800 cm^{-1} was previously assigned to the adsorption of CO at the metal/support interface (C bonded to the metal and O bonded to the support) [39], which makes evidence for a wide perimeter of the

boundary between Pd atoms and the highly dispersed CrO_x particles located whether on the surface of Pd nanoparticle or nearby its contact area with TiO_2 support.
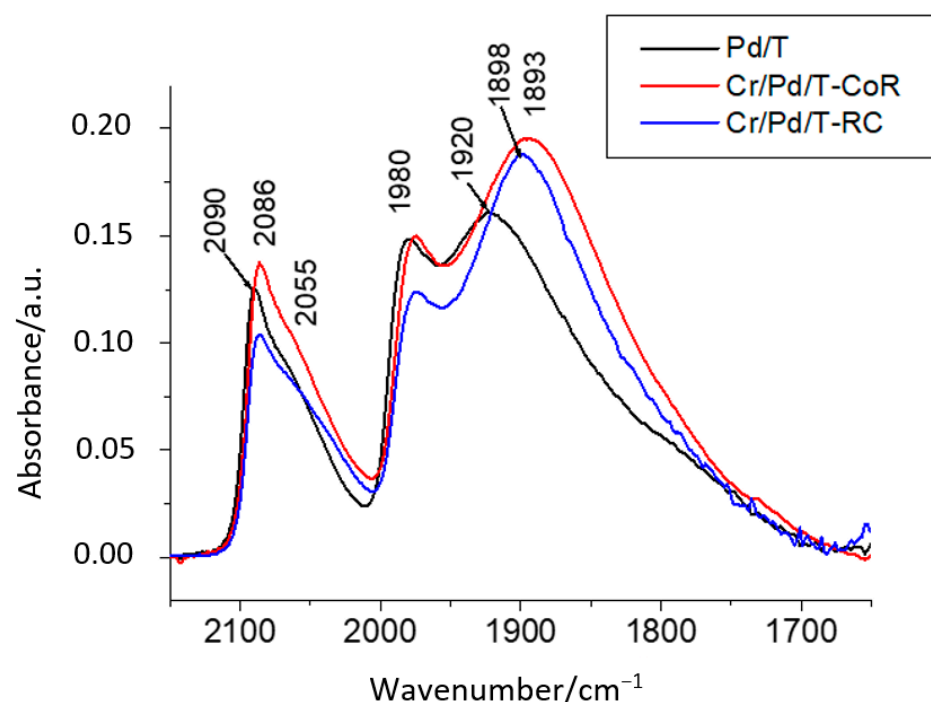

Figure 5. FTIR spectra of CO adsorbed at the pressure of 20 Torr on Pd/T, Cr/Pd/T-CoR, and Cr/Pd/T-RC samples.

The obtained values of irreversible CO chemisorption (n_{CO}), calculated Pd dispersity (γ_{Pd}), and crystallite size (hemisphere) are listed in Table 4. The overall value of CO chemisorption measured per gram of Pd decreased significantly after Cr deposition on the Pd nanoparticles, which can be due to the partial blocking of the sites of CO chemisorption by the deposited CrO_x species. The applied calculations give a slight decrease in Pd dispersion and the increased nanoparticle size. It should be mentioned that TEM studies show even larger average particle size, the difference in the particle size exhibits a partial character of covering the Pd nanoparticles with CrO_x solids. The Pd particle size and dispersity differed in an order of magnitude for the monometallic Pd samples prepared on SiO_2 and TiO_2 supports. Therefore, for the SiO_2-supported samples, the low Cr loadings can be due to the small number of sites for H_2 adsorption on the surface of the big Pd nanoparticles. Calculating the ratio of Cr ions in the solution to the surface Pd atoms, the value of 12 was obtained for Cr loading of 0.5 wt.%, which means the lack of adsorption sites for the achievement of such Cr loading. In the synthesized Pd/T sample, the Pd dispersity was considerably higher, and the mentioned ratio Cr:Pd drops to 2.7, opening the possibility of the higher Cr loading. A complete Cr withdrawal from solution was really found even during the preparation of the sample containing 1.1 wt.% Cr.

Table 4. Characterization of Pd nanoparticles.

Sample	Cr, %	Cr:Pd$_v$	n_{CO}, mmol g^{-1}$_{Pd}$	SF	S_{Pd}, m^2 g^{-1}	γ_{Pd}, %	Cr:Pd$_s$	d_{Pd}, nm	d_{TEM}, nm
Pd/S	0	-	0.26	1.80	24	5.3	-	21	22 (XRD)
Pd/T	0	-	2.1	1.80	180	40	-	2.8 ± 0.3	-
Cr/Pd/T-RC	0.36	0.74	1.9	1.82	160	37	1.9	3.1 ± 0.3	4.1 ± 0.9
Cr/Pd/T-CoR	0.36	0.74	1.9	1.81	160	36	1.9	3.1 ± 0.3	3.7 ± 0.9

Cr:Pd$_v$—the element atomic ratio in a sample; d_{Pd}—size of Pd nanoparticle; γ Pd—dispersion of Pd; SF—stoichiometric factor. RC—catalytic reduction by gaseous hydrogen; CoR—co-reduction with the supported polyhydroxo complexes of Pd (PHC).

2.2. TPR-H$_2$ Experiments

The XPS and FTIR of adsorbed CO techniques concern mostly with the surface composition, whereas a comprehensive picture of all the reducible species can be obtained with a TPR technique, whose results are depicted in Figures 6–8. The TPR curves for the initial Pd/support samples (Figures 6a and 7a) exhibited the negative peak of hydrogen release at 0–80 °C with the peak minimum at 55–60 °C, which is characteristic for the decomposition of the palladium β-hydride phase [40], indicating the presence of the Pd^0 nanoparticles. The negative peak of hydrogen release was observed previously for the mono- and bimetallic Pd samples synthesized via different redox procedures [20,21]. The β-PdH$_x$ phase can be formed during the preliminary low-temperature treatment of a sample with a hydrogen-containing flow at the beginning of the TPR experiment [12–14]. Besides this peak of hydrogen release, the weak overlapping peaks of hydrogen consumption were observed at temperature region from 200 °C to 500 °C for the Pd samples on both supports, and intensive hydrogen consumption from −100 °C to −50 °C was found only for the samples on TiO$_2$. Comprising these curves with the curves for Pd-PHC supported on γ-alumina and for the Pd^0 nanoparticles resulted from their reduction with hydrogen at room temperature (Figure 7d), one may conclude that (i) residual amount of Pd-PHC is negligible in the Pd/TiO$_2$ samples reduced with hydrogen at room temperature in the slurry; (ii) H$_2$ consumption below 0 °C is feature of very small (2.8 ± 0.3 nm) Pd^0 nanoparticles; (iii) the weak hydrogen consumption at a temperature higher than 250 °C may be due to reduction of some adsorbed species with product deletion from a sample, and, for the Pd/TiO$_2$ sample, a Pd-catalyzed reduction of support is possible as well.
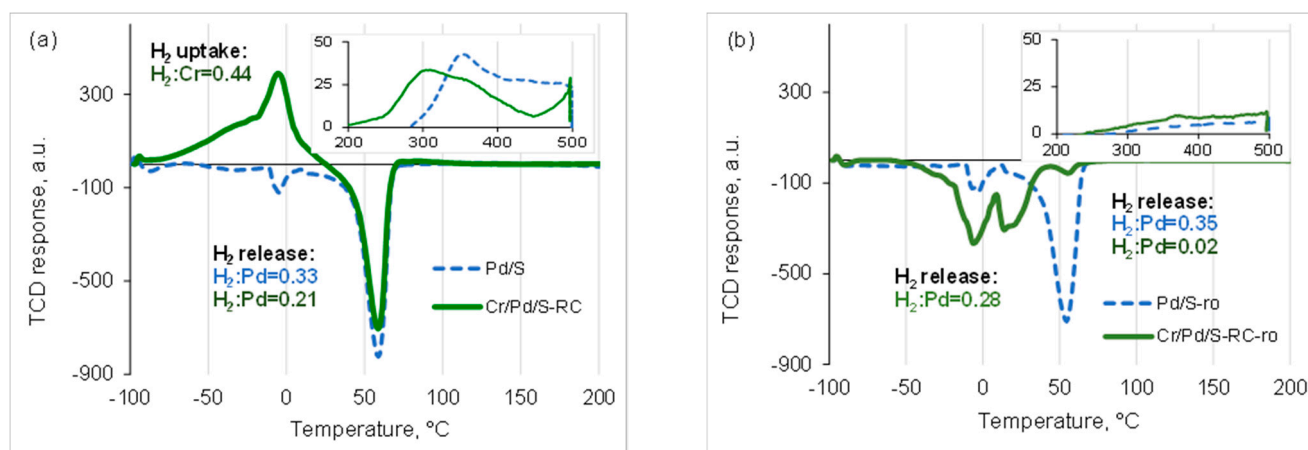

Figure 6. TPR curves of the samples: (**a**) initial Pd/S and Cr/Pd/S- RC samples and (**b**) the TPR-reduced samples after exposition to O$_2$ in the TPR system.

The redox deposition of CrO$_x$ species resulted in considerably decreased values of hydrogen release (Figure 8) for the samples both on Pd/S and Pd/T. These data indicate depositing the CrO$_x$ species on the Pd surface and their interaction. The curves and positions of the minimum hydrogen release correspond to the decomposition of palladium hydride in the initial palladium samples (Figures 6a and 7a). After reduction at 500 °C, two new intensive overlapping peaks of hydrogen release arise at lower temperatures instead of the previous one for SiO$_2$-supported bimetallic samples (Figure 6b), while the effect is weaker for TiO$_2$-supported samples (Figure 7). No similar changes in the TPR curves were observed earlier for bimetallic Pd catalysts. It should be mentioned that interaction between the metallic Pd particles and the transition metal ions was shown previously to result in the complete disappearance of hydrogen release [9,12–14], in the case of the catalyst preparation via other than redox procedures. The bimetallic samples prepared by the redox procedures, which were developed in the present work, retain the ability to release H$_2$ similar to the β-PdH$_x$ phase.
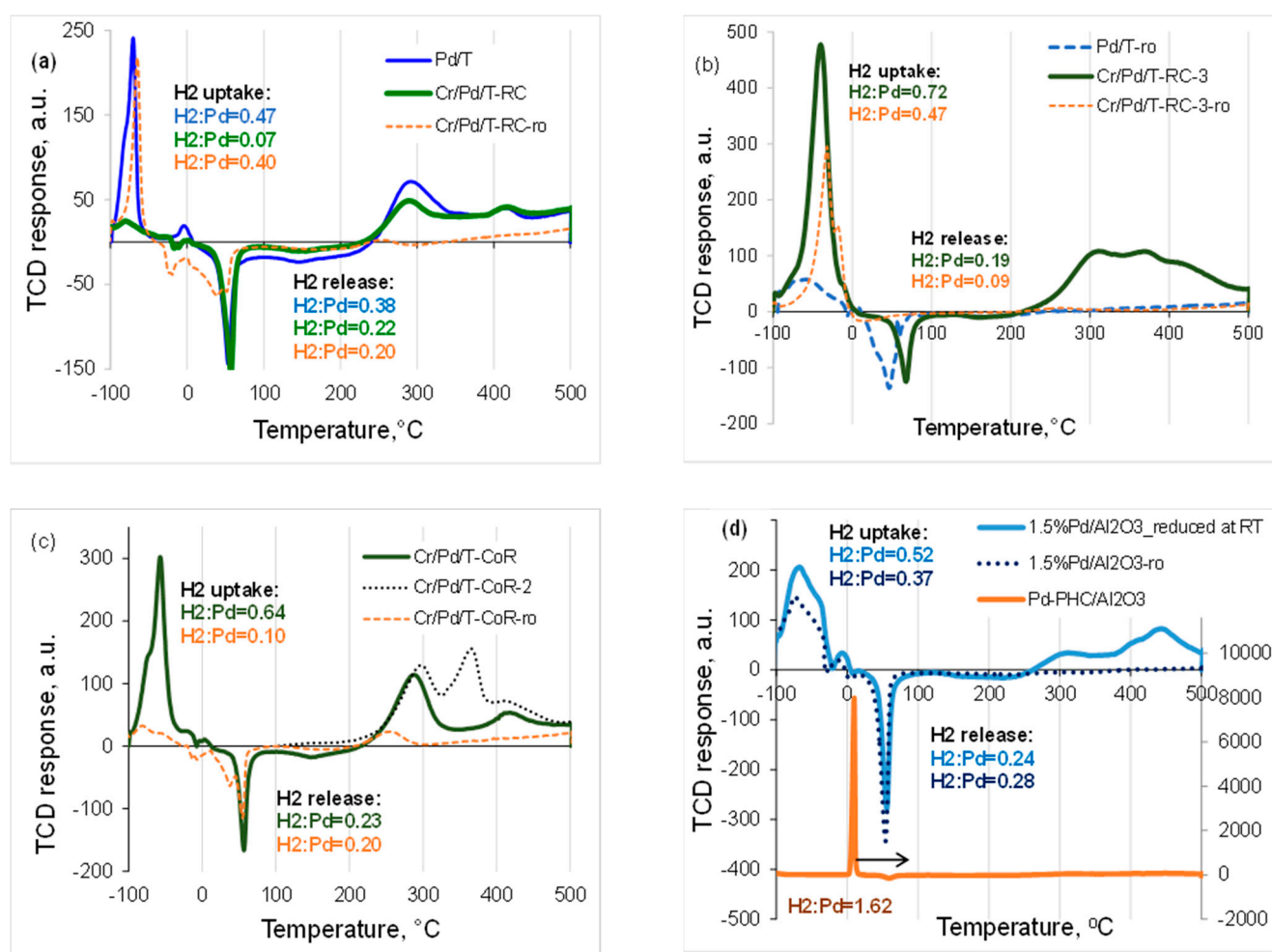
Figure 7. TPR curves of the initial samples and the TPR-reduced samples after exposition to O_2 in the TPR system (-ro): (**a**) Pd/T and Cr/Pd/T-RC samples; (**b**) Cr/Pd/T-RC-3 sample; (**c**) Cr/Pd/T-CoR samples; (**d**) Pd-PHC supported on γ-alumina and 1.5%Pd/Al$_2$O$_3$ sample reduced with H$_2$ at room temperature.
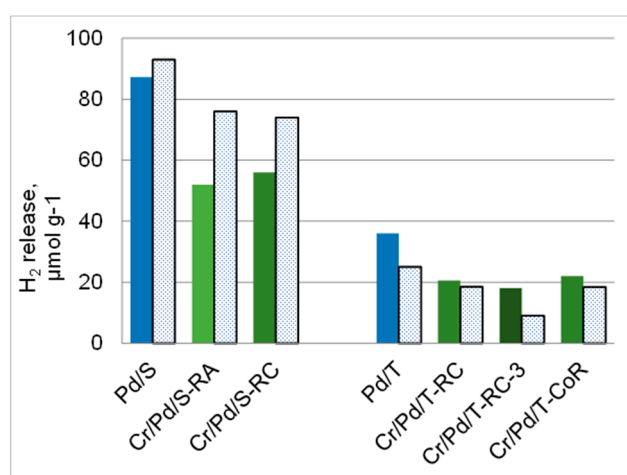

Figure 8. Hydrogen release due to β-PdH$_x$ decomposition for different samples before (solid fill) and after reduction at 500 °C (point fill).

Changes in the shape of TPR curves after redox CrO$_x$ deposition as compared with the curve of the monometallic Pd sample also evidenced the presence of CrO$_x$ species on the Pd surface. The curve shape depends on the nature of the support used and Cr

loading. The deposition of CrO_x on Pd/SiO_2 by RC procedure gave rise to a broad peak of H_2 consumption from -87 to $27\,°C$ with a sharp maximum at $-4\,°C$ (Figure 6a). The opposite effect of the disappearance of H_2 consumption peak was revealed in this region for the similar sample on the TiO_2 support (Figure 7a), whereas the triple increase of Cr loading resulted in a highly intensive sharp peak with a maximum at a considerably lower temperature both for initial and reduced at $500\,°C$ samples (Figure 7b). The peak in the same region was observed on the TPR curve of the initial Cr/Pd/T-CoR sample with a lower Cr loading, yet it disappeared after sample reduction (Figure 7c). Therefore, this consumption most likely has dissimilar origins for different samples. For Cr/Pd/S samples it may be attributed to an irreversible reduction of some CrO_x species deposited on the surface of large Pd nanoparticles, while for Cr/Pd/T samples the most probable explanation is Pd-catalyzed reversible reduction of CrO_x clusters located on the surface of Pd nanoparticles. The H_2 consumption in this region was reported earlier for Pd-Fe-O/SiO$_2$ samples, which were prepared by calcining the metal salt precursors co-precipitated on a silica gel support, and was attributed to the reduction of bimetallic Fe_2O_3–PdO nanoparticles [41,42], as well as for $FeO_x/Pd/SiO_2$ nanocatalysts obtained by redox deposition of iron oxide on Pd nanoparticles [21,43].

Weak H_2 consumption that was detected in the range of 300 to $500\,°C$ even for the initial Pd/S sample can be due to the Pd-catalyzed reduction of impurities in the commercial SiO_2 support, whereas the H_2 uptake values for the samples on TiO_2 correspond to the well-known reduction $Ti^{4+} \rightarrow Ti^{3+}$ catalyzed by Pd^0 in P-25 materials [44]. It should be mentioned that significant H_2 consumption peaks in the range of reversible reduction of CrO_x^{n-} weakly anchored to oxide support ($330–500\,°C$) [36,45] were revealed only for the Cr/Pd/T sample prepared by CoR procedure at Cr loading 0.43 mass % (Figure 7c).

The shape of the TPR curve for the sample on TiO_2 was changed as well after reduction-reoxidation treatment of the samples (Figure 7). The intensity of the negative peak at $55\,°C$ strongly decreased, and the minimum shifted to a lower temperature of $44\,°C$. Nevertheless, broad overlapping peaks of H_2 release were observed in the range -33 to $75\,°C$, and the total value of H_2 evolution decreased only slightly as compared with the initial Cr/Pd/T-RC sample (Figure 8). Such variation in the TPR curve may be due to the enlargement of Pd particles via the sintering of smaller particles. Yet the most surprising result was revealed in the range of negative temperatures: an intensive peak of hydrogen uptake from -90 to $-40\,°C$. The phenomenon is supposed to be caused by the incorporation of Cr^{n+} in the surface or subsurface layers of metallic Pd nanoparticles during a reduction in the TPR system at $500\,°C$.

Therefore, the procedure of sample synthesis seems to be the major reason for so strong a difference in the reduction behavior of bimetallic nanoparticles. The conditions of RA and RC procedures suppose deposition of CrO_x species only on the surface of preliminary formed Pd^0 nanocrystallites with no incorporation of Cr^{n+} ions into Pd^0 lattice. RC procedure makes possible deposition of larger Cr loading than RA procedure. During synthesis via the CoR procedure, the Pd^0 crystal growth proceeds via reduction of Pd-PHC nanoparticles modified with CrO_4^{2-} ions that are commonly accompanied by the formation of dislocations and grain boundaries making possible diffusion of ions from the surrounded liquid into the growing particles. Moreover, the possible dissolution of Pd-PHC may result in additional mass-transport of Pd^{2+} ions in solution resulting in the particle size decrease or growth. The reduced Pd moieties can adsorb H_2 causing a reduction of admixed ions and their encapsulation in the forming Pd nanoparticles.

2.3. Catalytic Activity

The results of experiments on testing the catalytic activity in the liquid-phase hydrogenation of phenylacetylene (PhA) revealed a strong influence of the CrO_x redox deposition on the catalytic properties of the catalysts prepared both on SiO_2 and TiO_2 supports. The catalytic activity of the SiO_2-supported Cr/Pd/S samples strongly depended on Cr loading and conditions of thermal treatment. For the samples with the maximum possible Cr con-

tent prepared via both RA and RC procedures, the activity was drastically lower than one of the initial Pd/S catalysts. If the complete conversion on the Pd/S sample was reached at 20 °C in 30 min, the Cr/Pd/S samples conversion was only 7% both on as-prepared samples and on the reduced at 500 °C samples. This fall in the activity may be due to the coverage of large Pd nanoparticles with CrO_x nanoparticles and possible blocking of the sites for PhA adsorption. It was recently shown that Pd terraces enable the high rate of acetylene bond hydrogenation to C=C bond on large Pd NPs of 20 nm in Pd/Al_2O_3 catalyst [46].

However, when the reaction temperature was increased to 45 °C, the activity of catalysts enhanced considerably, especially for the Cr/Pd/S sample with the ratio Cr:Pd$_v$ = 0.018 (Table 5). Both calcination in air and reduction in the hydrogen flow slightly enhanced its activity. Nevertheless, the activity and selectivity of the bimetallic samples were significantly lower than that of the initial Pd/S catalyst. It should be mentioned that inhibiting effect of CrO_x deposition on hydrogenation of double C=C bonds over a Pd catalyst was confirmed in the present work as well by the fact of more prolonged time required for complete hydrogenation of styrene (St), which appeared as a product of PhA hydrogenation, to ethylbenzene (EtB) over the Cr-modified catalysts. Hence, CrO_x deposition by RRA procedures on the large Pd nanoparticles, by any way, resulted in a considerable decrease in the catalytic activity of the Cr/Pd/S samples in selective PhA hydrogenation.

Table 5. The major results on the catalytic activity tests of Cr/Pd/S catalysts at 45 °C.

Sample	Cr, wt.%	Cr:Pd$_v$	T, °C	$r_{0(H2)}$	τ_{PhA}, min	S^{99}_{St}, %	τ_{St}, min
Pd/S	-	-	400 (H_2)	0.58	3.5	91	3
Cr/Pd/S-RA	0.026	0.018	60 (air)	0.24	11	78	10
Cr/Pd/S-RA	0.026	0.018	400 (air)	0.40	5	73	6
Cr/Pd/S-RA	0.026	0.018	400 (H_2)	0.33	6	81	8
Cr/Pd/S-RA	0.26	0.18	500 (H_2)	0.051	72	73	180

T—the temperature of catalyst thermal treatment; $r_{0(H2)}$—initial rate of hydrogen consumption ($mol_{H2}\ mol_{Pd}^{-1}\ s^{-1}$) during reaction; τ- time of complete conversion of PhA and St respectively; S^{99}_{St}—selectivity to styrene at almost complete PhA conversion. RA–reduction by preadsorbed hydrogen

The influence of CrO_x deposition on the smaller Pd nanoparticles in Cr/Pd/T samples was revealed to be more complicated and dissimilar, depending on the procedure used and Cr loading. Comparing the catalytic activity and selectivity for the $Cr/Pd/TiO_2$ samples with almost equal Cr contents and Cr/Pd$_v$ ratios (Figure 9, Table 6) allow us to conclude that their catalytic properties strongly depend on the reduction behavior governed by the preparation procedure. The sample Cr/Pd/T-RC, which showed no H_2 consumption below 20 °C in the TPR run, exhibited higher catalytic activity and selectivity than the parent Pd catalyst in the hydrogenation of triple to double carbon bonds in PhA. Whereas there was a significant decrease in the catalytic activity and selectivity for the sample Cr/Pd/T-CoR, the TPR curve profile showed the large H_2 uptake at temperatures below 0 °C. The chemical composition, the calculated sizes of Pd nanoparticles, Cr/Pd$_s$ ratios, the profiles and values of H_2 evolution due to β-PdH_x decomposition for these samples, Pd electronic state are close, yet FTIR spectra of adsorbed CO exhibit a significant difference in the adsorption properties of the Pd surface sites. Therefore, the influence of the sample synthesis procedure seems the major reason for so strong a difference in the reduction and catalytic behavior.
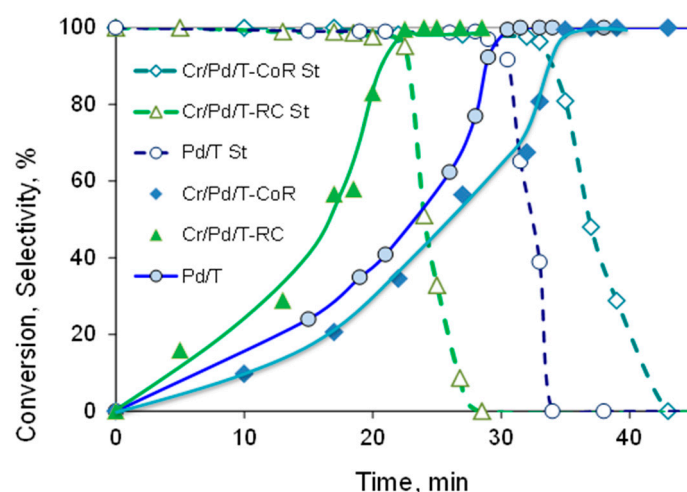
Figure 9. Time dependence of the PhA conversion (solid lines) and selectivity to St (dashed lines) for the initial Pd/TiO_2 and redox prepared $Cr/Pd/TiO_2$ catalysts with Cr loading of 0.36%.

Table 6. The major results on the catalytic activity tests for the Cr/Pd/T catalysts at 20 °C.

Sample	Cr, % wt.	Cr:Pd$_v$	$r_{0(H2)}$[c]	τ_{PhA}[a], min	S^{99}_{St} [b], %	τ_{St}[a], min
Pd/T	-	-	0.14	32	92	2.5
Cr/Pd/T-RC	0.36	0.74	0.45	24	95	10
Cr/Pd/T-RC-2	0.72	1.50	0.70	9	83	7
Cr/Pd/T-RC-3	1.10	2.20	0.56	9	85	11
Cr/Pd/T-CoR	0.36	0.74	0.14	35	81	6

$r_{0(H2)}$—initial rate of hydrogen consumption ($mol_{H2}\ mol_{Pd}^{-1}\ s^{-1}$) during reaction; τ—time of complete conversion of PhA and St respectively; S^{99}_{St}—selectivity to styrene at almost complete PhA conversion. RC—catalytic reduction by gaseous hydrogen; CoR—co-reduction with the supported polyhydroxo complexes of Pd (PHC).

During synthesis via the CoR procedure, the formation of Pd^0 crystallites initially proceeds via reduction of Pd-PHC nanoparticles modified with CrO_4^{2-} ions, and as a result, the Cr^{n+} ions may be blocked. The conditions of the RC procedure suppose deposition of CrO_x species only on the surface of preliminary formed Pd^0 crystallites with no incorporation of Cr^{n+} ions into Pd^0 lattice. The boundaries of CrO_x species with the surface of Pd nanoparticles, as well as with TiO_2 support—the presence of which partly confirmed by poorly resolved bands below 1850 cm^{-1} observed as tailing in DRIFT-CO spectra of Cr/Pd/T samples—may serve as additional sites for PhA adsorption thus enhancing the catalytic activity, and time of complete PhA conversion decreased with Cr loading up to 0.72% (Figure 10a). At the same time, the initial rate of H_2 consumption considerably increased as compared with the Pd/T sample (Table 6) that indicated the enhanced activation of H_2 molecules on the surface of bimetallic nanoparticles. It should be mentioned, that selectivity to St at complete PhA conversion was the highest for the sample with Cr loading 0.36% (Figure 10b).

To sum up, the highly dispersed bimetallic nanoparticles on TiO_2 support that were synthesized via the catalytic reduction by gaseous hydrogen (RC procedure) are considerably more active than the initial Pd catalyst in the reaction of the selective liquid-phase hydrogenation of phenylacetylene. It was also shown that the same procedure of parent Pd modification with CrO_4^{2-} ions resulted in irreversible catalytic effect for SiO_2 and TiO_2 supported Pd NPs characterized by different mean Pd NPs sizes.
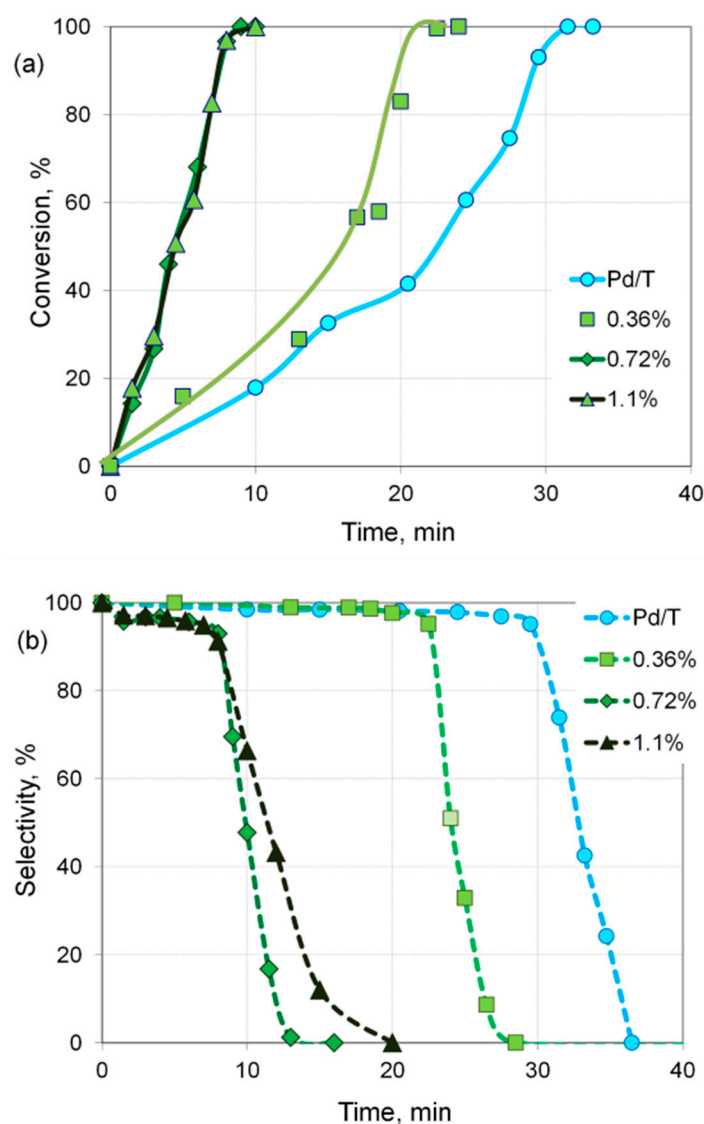
Figure 10. Time dependence of (**a**) PhA conversion and (**b**) selectivity to St for the initial Pd/TiO_2 and redox prepared Cr/Pd/T-RC catalysts with different Cr loading.

3. Experimental

3.1. Catalyst Synthesis

The deposition of Pd^0 nanoparticles on the surface of carriers was performed via deposition of Pd precursor nanoparticles on the surface followed by a reduction to Pd^0 nanoparticles with hydrogen. The starting $3\%Pd/SiO_2$ material was synthesized by incipient wetness impregnation of commercial silica gel (ChimMed, Russia, KSKG, S_{BET} = 98 m^2 g^{-1}, D_{pore} = 26 nm) with an aqueous solution of $[Pd(NH_3)_4]Cl_2$, followed by drying and reduction in a hydrogen flow at 400 °C. This temperature is known to be sufficient for the reduction of $PdCl_2$ to Pd^0 [47]. The starting $1\%Pd/TiO_2$ material was synthesized by the method of deposition-precipitation of Pd polyhydroxo-complexes (PHC) on the titania support followed by reduction of PHC to metallic nanoparticles with hydrogen in a slurry as described previously [20]. The method includes (i) the preparation of an aqueous slurry of TiO_2 powder in a preliminary prepared solution that contained H_2PdCl_4 and Na_2CO_3 in a ratio 1:2.0 ± 0.1 at 4 °C; (ii) deposition of Pd-PHC by keeping the stirred slurry at 4°C and then at 23 °C for 1 h, heating the slurry to 60°C and maintaining this temperature for 4 h; (iii) reduction of thus supported Pd-PHC with H_2 for 2 h in the slurry cooled to 23 °C; (iv) separation, washing, and drying the sample under vacuum of 40 mbar at 40 °C using

a rotary evaporator. The commercial TiO_2 powder (P-25 AEROXIDE, Evonic, Germany, $S_{BET} = 57$ m^2 g^{-1}, nonporous, d$_{NPs} = 21$ nm) was used as a support.

The Cr/3%Pd/SiO$_2$ materials were prepared using the RA and RC procedures of reduction with adsorbed hydrogen. According to the RA procedure, a 3%Pd/SiO$_2$ sample just after reduction was cooled to room temperature in a hydrogen flow, and then a chromic acid solution of the required concentration (H$_2$CrO$_4$ aq, Reachim, Russia) was poured into a quartz reactor to the sample with no exposition to air. The ratio of the added solution volume to the water capacity of the Pd sample was 1.5:1. The obtained suspension was periodically shaken and kept at room temperature for a certain time. The sample was separated by centrifuging, and a solid was dried on a rotary evaporator at 40 mbar and 60 °C. The residual CrO$_4{}^{2-}$ content in the separated solution was determined by volumetric titration with KI solution. Preparation by the RC procedure was performed as follows. The preliminary reduced 3%Pd/SiO$_2$ sample (0.22 g) was placed in a two-neck round-bottom flask (250 mL), and 30 mL of a chromic acid solution was added forming a slurry with pH = 4.4. After purging the flask with H$_2$, the slurry was stirring for the required time under a weak H$_2$ flow at 23 °C. The completeness of Cr precipitation was checked by probing with KJ and starch solutions. The complete Pd and Cr^{3+} deposition was also confirmed by EDS elemental analysis (Table S1). The optimal solution concentrations and time of reduction required for complete precipitation were found in the preliminary experiments, and their values are listed in Table 1. The sample was separated by centrifuging, and the pH of the separated solution was 8.3. Then the sample was triple washed with double deionized water. The obtained solid was dried using a rotary evaporator at 40 mbar and 60 °C. The samples were denoted as "Cr/Pd/S-RA" and "Cr/Pd/S-RC", correspondingly.

The Cr/1%Pd/TiO$_2$ materials were prepared according to the RC procedure similar to the one used in this work for the preparation of Cr/Pd/S-RC samples, as well as by the CoR procedure similar to the one described in [20]. According to the RC procedure, the washed sample 1%Pd/TiO$_2$ was introduced in a flask poured with a proper amount of a chromic acid solution of required concentration (H$_2$CrO$_4$ aq). After purging the flask with H$_2$, the slurry was stirred for 3–5 h under a weak H$_2$ flow at 23 °C until the absence of Cr^{6+} in a probe of solution. After separation from the solution, the sample was washed with double distilled water (pH = 6.3). The CoR procedure supposed modification of 1%Pd/TiO$_2$ synthesis by the introduction of chromic acid in the slurry before the step of reduction of supported Pd-PHC. The detailed scheme of preparation of Pd-PHC/TiO$_2$ as well as 1%Pd/TiO$_2$ samples is depicted in [20]. The samples were marked as "Cr/Pd/T-RC" and "Cr/Pd/T-CoR", correspondingly. The Cr mass content in the samples is presented in Table 1.

When working with chromic acid, contact with eyes and skin was avoid. A self-suction respirator, acid-proofing rubber gloves, security coat, chemical-resistant protective glasses were used.

3.2. Catalyst Characterization

The SEM observations were carried out using Hitachi SU8000 (Hitachi, Tokyo, Japan) field-emission scanning electron microscope (FE-SEM). Images were acquired in secondary electron mode at 2 kV accelerating voltage. To gain SEM images, before measurements the samples were mounted on a 25 mm aluminum specimen stub, fixed by conductive plasticine-like adhesives, and coated with a thin film (15 nm) of carbon. The morphology of the samples was studied considering the possible influence of carbon coating on the surface. EDS-SEM studies were carried out using Oxford Instruments X-max 80 EDS (High Wycombe, UK) system at 20 kV accelerating voltage.

Morphology of the samples and the Pd particle size distribution were studied using Hitachi HT7700 (Tokyo, Japan) transmission electron microscope. Images were acquired in bright-field TEM mode at 100 kV accelerating voltage. A target-oriented approach was utilized for the optimization of the analytic measurements [48]. Before measurements, the samples were deposited on the 3 mm carbon-coated copper grids from suspension in

isopropanol. The average particle size (d_{av}) of Pd NPs was calculated as $d_{av} = \Sigma n_i d_i/n$, where n_i represents the number of particles with the diameter d_i, n is the total number of calculated particles. The total number of calculated particles for each sample was 300, and at least 7 TEM images were used to obtain the statistics of the particle size distribution. Calculations were made using Digimizer Image Analysis Software.

X-ray photoelectron spectra of the $CrO_x/Pd/TiO_2$ samples were recorded on a PHI5000 VersaProbeII (ULVAC-PHI, Inc. 2500 Hagisono, Chigasaki, Kanagawa, Japan) spectrometer. The spectrometer was preliminarily calibrated by the BE of the Au 4f level = 83.96 eV and Cu 2p3/2 = 932.62 eV. Correction of BE scale was performed based on a peak position for Pd $3d_{5/2}$ doublet 1-1′ shifted to set 335,1 eV, BE of Ti 2p3 being 459,0 eV. The monochromatic Kα radiation of the Al anode (1486.6 eV) at a power of 50 W was used as an X-ray source. The high-resolution spectra were recorded with a pass energy of 23.5 eV, spot size of 200 μm, step size of 0.2 eV. Non-linear least-squares fitting was performed using the Gauss-Lorentz algorithm including asymmetry for doublet 1-1′ Pd 3d.

Infrared spectra were recorded on a Nicolet Protege 360 (Nicolet Instrument Corporation, Madison, WI, USA) spectrophotometer in transmittance mode (spectral resolution 4 cm^{-1}). Powdered materials were pressed into self-supporting wafers (15–25 mg cm^{-2}) and placed in a vacuum infrared quartz cell equipped with CaF_2 windows. The IR spectra of carbon monoxide adsorbed on the samples (20 Torr) were measured after (i) evacuation of the samples for 1 h at 40 °C, (ii) subsequent reduction in hydrogen at 22 °C at static conditions for 1h (two cycles of exposure of a specimen to 100 Torr of H_2 for 30 min with evacuation to 10^{-4} Torr in-between the H_2 exposures) (iii) final evacuation at 40 °C for 1 h. Carbon monoxide was adsorbed on the reduced samples at the equilibrium pressure of 20 Torr at ambient temperature. The spectra given herein are difference spectra with the spectra of the samples before CO adsorption as a background.

Since X-ray phase analysis of 1%Pd/TiO$_2$ samples on P-25 is not informative [44], the size (d) and the dispersion (γ) of supported metallic Pd nanoparticles were calculated based on Sinfelt method [49]—the value of irreversible CO chemisorption measured at 35 °C using a Micromeritics ASAP 2020 Plus instrument (Micromeritics, Norcross, GA, USA). Before chemisorption measurement, the $CrO_x/Pd/TiO_2$ sample was evacuated at 40 °C for 60 min, reduced in a hydrogen flow at 25 °C for 40 min, and evacuated at 35 °C for 90 min. to a pressure of 10^{-3} mm Hg. The chemisorption on Pd was obtained by subtracting the support contribution from the total. After evacuating the sample, the CO adsorption isotherm was measured (8 points in the range of 100–450 mm Hg.) Then CO is evacuated for 30 min and the repeated isotherm was measured. The intersection of the linear region of the difference isotherm with the ordinate axis is taken as the amount of chemisorption. The dispersion was calculated taking into account the stoichiometric factor (SF) calculated from the data of the IR spectra of adsorbed CO as a ratio of signal areas for linear absorbed CO and bridge CO bands.

The materials were studied by the TPR-H$_2$ method using the setup described in [21,42,50] and the similar two-stage procedure The TPR-H$_2$ studies included (1) TPR-H$_2$ run from −100 °C up to 500 °C followed by reduction at this temperature until H$_2$ consumption ceased; (2) in situ exposition to oxygen at room temperature; and (3) TPR-H$_2$ run of the reoxidized sample. The highest reduction temperature of 500 °C was selected based on the results of our previous studies on the reducibility of the systems CrO_x/TiO_2 [51] and $CrO_x/Pd/TiO_2$ [20], as well as on the data published for CrO_3/SiO_2 [36]. Before TPR runs the samples (0.10 ± 0.01 g of fraction 0.25–0.35 mm) were kept in an Ar flow at 40 °C for 1.5 h, then they were cooled to −100 °C. At this temperature, the flow was switched to the reducing gas, and the sample was maintained at these conditions until the baseline became stable (about 30 min). Then the samples were heated from −100 °C to 500 °C with a heating rate of 10 °C min^{-1} in a flow (30 mL min^{-1}) of reducing mixture (5% H$_2$ in Ar) and reduced at 500 °C until H$_2$ consumption became negligible. The reduced sample was cooled down to room temperature in the Ar flow and then was kept in a (5% O$_2$ in He) flow (40 mL min^{-1}) in the TPR system for 2 h and further in this oxidizing medium overnight.

Thus treated sample was then reduced again in the TPR run. A thermal conductivity detector (TCD) was used in order to record changes in H_2 concentration and to measure H2 uptake and release. Before TCD, the reduction products were passing through a cold trap at $-100\,°C$ to remove H_2O. Hydrogen consumption (release) was determined based on the measured values of area for peaks on the time-dependence TCD curves and the preliminary calibration with CuO (Aldrich-Chemie GmbH, 99%, Darmstadt, Germany) pretreated in an Ar flow at 300 °C. The presented TPR profiles were normalized per 1 g of material.

3.3. Catalytic Activity Test

The catalytic behavior of the prepared bimetallic and monometallic Pd nanoparticles was characterized in the model reaction of the liquid-phase hydrogenation of phenylacetylene (PhA) with molecular hydrogen. The catalytic activity was studied at 20 °C and atmospheric hydrogen pressure in a glass reactor in a batch mode according to the procedure reported previously in [21,41,52] as follows. A three-neck glass reactor was poured with ethanol (19 mL) and the catalyst sample (30 mg) was added. The reactor was connected with an H_2 supplying system, and after purging with an H_2 flow, was vigorously shaken for 30 min (until H_2 consumption stopped). Then undecane (internal standard) and PhA were introduced in the reactor using syringes and shaking continued. The molar ratio PhA:Pd was 290 and 480 for SiO_2- and TiO_2-supported samples correspondingly, PhA concentration in solution was 0.13 mol L^{-1}. The time dependences of the PhA and product concentrations, as well as H_2 consumption, were determined. Samples of the reaction mixture were analyzed by GLC with an internal standard method. Only styrene (St) and ethylbenzene (EtB) were detected as reaction products, and the carbon balance was better than 99%. The results were shown in a common way to take into account the time dependences of the PhA conversion and selectivity to the products.

4. Conclusions

The preparation procedures based on reduction with H_2 preadsorbed on Pd^0 nanoparticles make possible deposition of CrO_x species from aqueous solutions of chromic acid at ambient conditions on the surface of Pd^0 nanoparticles supported on the commercial oxide materials. During further reduction in a hydrogen-contained gas flow, Cr^{n+} cations seem to diffuse in bulk, and their oxidation with O_2 from gas is retarded at room temperature. SEM, EDS-SEM, TEM, XPS, FTIR of adsorbed CO, and CO chemisorption studies were performed to characterize the morphology, nanoparticle size, element, and particle distribution, as well as electronic state of deposited metals in the obtained catalysts. The redox behavior of novel materials prepared via the novel procedures of the redox deposition of CrO_x species on the metallic Pd nanoparticles has been studied using the method of temperature-programmed reduction with hydrogen (TPR-H_2). The TPR curve profiles obtained in this work indicate a strong interaction between the deposited CrO_x species and Pd^0, as well as confirming the deposition of CrO_x species on the surface of Pd nanoparticles, thus testifying to the availability of the surface of the modified Pd nanoparticles for H_2 adsorption with the formation of β-PdH_x both in the initial and reduced samples. The decrease in the temperature of β-PdH decomposition from $-11°C$–$+80\,°C$ to $-60\,°C$–$+40\,°C$, as well as the intensive hydrogen consumption in the temperature range of -50 to $+40\,°C$ (Cr/Pd/SiO_2) and -90 to $-40\,°C$ (Cr/Pd/TiO_2), have been shown for the first time for the oxide-supported bimetallic Pd materials. Redox-deposition of CrO_x species on Pd^0 nanoparticles influences the catalytic properties of palladium catalysts in hydrogenation of unsaturated C-C bonds, and the effects depend on the Cr/Pd ratio, the preparation procedure, and the size of Pd NPs, as well as support in the initial Pd catalyst. The highly dispersed bimetallic nanoparticles on TiO_2 support that were synthesized via the catalytic reduction by gaseous hydrogen (RC procedure) were considerably more active than the initial Pd catalyst in the reaction of selective liquid-phase hydrogenation of phenylacety-

lene to styrene at room temperature and atmospheric hydrogen pressure, and consecutive hydrogenation of triple C≡C to double C=C and C-C bond proceeds.

References

1. Arnold, H.; Döbert, F.; Gaube, J. Hydrogenation reactions. In *Handbook of Heterogeneous Catalysis*, 2nd ed.; Ertl, G., Knözinger, H., Schüth, F., Weitkamp, J., Eds.; Wiley-VCH Verlag GmbH&Co. KGaA: Weinheim, Germany, 2008; Volume 7, pp. 3266–3359.
2. Nasrollahzadeh, M.; Sajjadi, M.; Shokouhimehr, M.; Varma, R.S. Recent Developments in Palladium (Nano)Catalysts Supported on Polymers for Selective and Sustainable Oxidation Processes. *Coord. Chem. Rev.* **2019**, *397*, 54–75. [CrossRef]
3. Trzeciak, A.M.; Augustyniak, A.W. The Role of Palladium Nanoparticles in Catalytic C–C Cross-Coupling Reactions. *Coord. Chem. Rev.* **2019**, *384*, 1–20. [CrossRef]
4. Alonso, D.; Baeza, A.; Chinchilla, R.; Gómez, C.; Guillena, G.; Pastor, I.; Ramón, D. Solid-Supported Palladium Catalysts in Sonogashira Reactions: Recent Developments. *Catalysts* **2018**, *8*, 202. [CrossRef]
5. Xu, X.; Shuai, K.; Xu, B. Review on Copper and Palladium Based Catalysts for Methanol Steam Reforming to Produce Hydrogen. *Catalysts* **2017**, *7*, 183. [CrossRef]
6. Louis, C.; Delannoy, L. Selective hydrogenation of polyunsaturated hydrocarbons and unsaturated aldehydes over bimetallic catalysts. In *Advances in Catalysis*; Elsevier: Amsterdam, The Netherlands, 2019; Volume 64, pp. 1–88, ISBN 978-0-12-817099-1.
7. Dasgupta, A.; Rioux, R.M. Intermetallics in Catalysis: An Exciting Subset of Multimetallic Catalysts. *Catal. Today* **2019**, *330*, 2–15. [CrossRef]
8. Marakatti, V.S.; Peter, S.C. Synthetically Tuned Electronic and Geometrical Properties of Intermetallic Compounds as Effective Heterogeneous Catalysts. *Prog. Solid State Chem.* **2018**, *52*, 1–30. [CrossRef]
9. Coq, B.; Figueras, F. Bimetallic Palladium Catalysts: Influence of the Co-Metal on the Catalyst Performance. *J. Mol. Catal. Chem.* **2001**, *173*, 117–134. [CrossRef]
10. Mashkovsky, I.S.; Markov, P.V.; Bragina, G.O.; Baeva, G.N.; Rassolov, A.V.; Bukhtiyarov, A.V.; Prosvirin, I.P.; Bukhtiyarov, V.I.; Stakheev, A.Y. PdZn/α-Al$_2$O$_3$ Catalyst for Liquid-Phase Alkyne Hydrogenation: Effect of the Solid-State Alloy Transformation into Intermetallics. *Mendeleev Commun.* **2018**, *28*, 152–154. [CrossRef]
11. Mashkovsky, I.S.; Smirnova, N.S.; Markov, P.V.; Baeva, G.N.; Bragina, G.O.; Bukhtiyarov, A.V.; Prosvirin, I.P.; Stakheev, A.Y. Tuning the Surface Structure and Catalytic Performance of PdIn/Al$_2$O$_3$ in Selective Liquid-Phase Hydrogenation by Mild Oxidative-Reductive Treatments. *Mendeleev Commun.* **2018**, *28*, 603–605. [CrossRef]
12. Pinna, F.; Selva, M.; Signoretto, M.; Strukul, G.; Boccuzzi, F.; Benedetti, A.; Canton, P.; Fagherazzi, G. Pd-Fe/SiO2 Catalysts in the Hydrogenation of 2,4-Dinitrotoluene. *J. Catal.* **1994**, *150*, 356–367. [CrossRef]
13. Juszczyk, W.; Pielaszek, J.; Karpiński, Z.; Pinna, F. Reaction of 2,2-Dimethylpropane with Dihydrogen over Silica-Supported PdFe Catalysts. *Appl. Catal. Gen.* **1996**, *144*, 281–291. [CrossRef]
14. Yang, J.; Li, S.; Zhang, L.; Liu, X.; Wang, J.; Pan, X.; Li, N.; Wang, A.; Cong, Y.; Wang, X.; et al. Hydrodeoxygenation of Furans over Pd-FeOx/SiO$_2$ Catalyst under Atmospheric Pressure. *Appl. Catal. B Environ.* **2017**, *201*, 266–277. [CrossRef]
15. Redina, E.A.; Kirichenko, O.A.; Shesterkina, A.A.; Kustov, L.M. Unusual Behavior of Bimetallic Nanoparticles in Catalytic Processes of Hydrogenation and Selective Oxidation. *Pure Appl. Chem.* **2020**, *92*, 989–1006. [CrossRef]
16. Shesterkina, A.A.; Kustov, L.M.; Strekalova, A.A.; Kazansky, V.B. Heterogeneous Iron-Containing Nanocatalysts—Promising Systems for Selective Hydrogenation and Hydrogenolysis. *Catal. Sci. Technol.* **2020**, *10*, 3160–3174. [CrossRef]
17. Ouchaib, T.; Moraweck, B.; Massardier, J.; Renouprez, A. Charcoal Supported Palladium and Palladium-Chromium Catalysts: A Comparison in the Hydrogenation of Dienes with Silica Supported Metals. *Catal. Today* **1990**, *7*, 191–198. [CrossRef]

18. Borgna, A. New Supported Palladium-Chromium Catalysts: Characterization and Catalytic Properties. *J. Catal.* **1991**, *128*, 99–112. [CrossRef]

19. Hu, L.; Xia, G.; Qu, L.; Li, M.; Li, C.; Xin, Q.; Li, D. The Effect of Chromium on Sulfur Resistance of Pd/HY–Al$_2$O$_3$ Catalysts for Aromatic Hydrogenation. *J. Catal.* **2001**, *202*, 220–228. [CrossRef]

20. Kustov, L.M.; Tarasov, A.L.; Kirichenko, O.A. Microwave-Activated Dehydrogenation of Perhydro-*N*-Ethylcarbazol over Bimetallic Pd-M/TiO$_2$ Catalysts as the Second Stage of Hydrogen Storage in Liquid Substrates. *Int. J. Hydrog. Energy* **2017**, *42*, 26723–26729. [CrossRef]

21. Kirichenko, O.; Strekalova, A.; Kapustin, G.; Shesterkina, A.; Redina, E.; Kustov, L. Redox Behavior of Novel FeOx/Pd/SiO$_2$ Catalytic Nanomaterials. *J. Therm. Anal. Calorim.* **2019**, *138*, 1913–1922. [CrossRef]

22. Richard, F.C.; Bourg, A.C.M. Aqueous Geochemistry of Chromium: A Review. *Water Res.* **1991**, *25*, 807–816. [CrossRef]

23. Pfennig, A. Kirk-Othmer Encyclopedia of Chemical Technology, Vol. 1. Herausgeg. von J. I. Kroschwitz und M. Howe-Grant. John Wiley & Sons, New York—Chichester—Toronto 1991.4. Aufl., XXXII, 1087 S., zahlr. Abb. u. Tab., geb., Subskriptionspreis US-$ 225,-. *Chem. Ing. Tech.* **1992**, *64*, 1134. [CrossRef]

24. Barbier, J. *Handbook of Heterogeneous Catalysis*; Ertl, G., Knözinger, H., Weitkamp, J., Eds.; Wiley-VCH: Weinheim, Germany, 1997; p. 257.

25. Barbier, J. Redox methods for preparation of bimetallic catalysts. In *Preparation of Solid Catalysts*; Ertl, G., Knozinger, H., Weitkamp, J., Eds.; WILEY-VCH Verlag GmbH: Weinheim, Germany, 1999; pp. 526–540.

26. Redina, E.A.; Kirichenko, O.A.; Greish, A.A.; Kucherov, A.V.; Tkachenko, O.P.; Kapustin, G.I.; Mishin, I.V.; Kustov, L.M. Preparation of Bimetallic Gold Catalysts by Redox Reaction on Oxide-Supported Metals for Green Chemistry Applications. *Catal. Today* **2015**, *246*, 216–231. [CrossRef]

27. Kosmulski, M. PH-Dependent Surface Charging and Points of Zero Charge. IV. Update and New Approach. *J. Colloid Interface Sci.* **2009**, *337*, 439–448. [CrossRef] [PubMed]

28. Huang, S.; Wang, J.; Li, Y.; Tang, J.; Zhang, X. Microstructure Characterization and Formation Mechanism of Colloid Palladium for Activation Treatment on the Surface of PPTA Fibers. *Appl. Surf. Sci.* **2020**, *516*, 146134. [CrossRef]

29. Guo, J.; Mao, L.; Zhang, J.; Feng, C. Role of Cl$^-$ Ions in Photooxidation of Propylene on TiO$_2$ Surface. *Appl. Surf. Sci.* **2010**, *256*, 2132–2137. [CrossRef]

30. John, F.; Moulder William, F.; Stickle Peter, E.; Sobol Kenneth, D. *Handbook of X-ray Photoelectron Spectroscopy*; Chastain, J., Ed.; Perkin-Elmer: Eden Prairie, MN, USA, 1992; Volume 118.

31. Aronniemi, M.; Sainio, J.; Lahtinen, J. Chemical State Quantification of Iron and Chromium Oxides Using XPS: The Effect of the Background Subtraction Method. *Surf. Sci.* **2005**, *578*, 108–123. [CrossRef]

32. Vasconcelos Borges Pinho, P.; Chartier, A.; Moussy, J.-B.; Menut, D.; Miserque, F. Crystal Field Effects on the Photoemission Spectra in Cr$_2$O$_3$ Thin Films: From Multiplet Splitting Features to the Local Structure. *Materialia* **2020**, *12*, 100753. [CrossRef]

33. Liu, B.; Šindelář, P.; Fang, Y.; Hasebe, K.; Terano, M. Correlation of Oxidation States of Surface Chromium Species with Ethylene Polymerization Activity for Phillips CrOx/SiO$_2$ Catalysts Modified by Al-Alkyl Cocatalyst. *J. Mol. Catal. Chem.* **2005**, *238*, 142–150. [CrossRef]

34. Xu, L.; Zuo, Y.; Tang, J.; Tang, Y.; Ju, P. Chromium–Palladium Films on 316L Stainless Steel by Pulse Electrodeposition and Their Corrosion Resistance in Hot Sulfuric Acid Solutions. *Corros. Sci.* **2011**, *53*, 3788–3795. [CrossRef]

35. Keller, P.; Strehblow, H.-H. XPS Investigations of Electrochemically Formed Passive Layers on Fe/Cr-Alloys in 0.5 M H$_2$SO$_4$. *Corros. Sci.* **2004**, *46*, 1939–1952. [CrossRef]

36. Liotta, L.F.; Venezia, A.M.; Pantaleo, G.; Deganello, G.; Gruttadauria, M.; Noto, R. Chromia on Silica and Zirconia Oxides as Recyclable Oxidizing System: Structural and Surface Characterization of the Active Chromium Species for Oxidation Reaction. *Catal. Today* **2004**, *91–92*, 231–236. [CrossRef]

37. Lear, T.; Marshall, R.; Antonio Lopez-Sanchez, J.; Jackson, S.D.; Klapötke, T.M.; Bäumer, M.; Rupprechter, G.; Freund, H.-J.; Lennon, D. The Application of Infrared Spectroscopy to Probe the Surface Morphology of Alumina-Supported Palladium Catalysts. *J. Chem. Phys.* **2005**, *123*, 174706. [CrossRef] [PubMed]

38. Garbowski, E.; Feumi-Jantou, C.; Mouaddib, N.; Primet, M. Catalytic Combustion of Methane over Palladium Supported on Alumina Catalysts: Evidence for Reconstruction of Particles. *Appl. Catal. Gen.* **1994**, *109*, 277–291. [CrossRef]

39. Boujana, S.; Demri, D.; Cressely, J.; Kiennemann, A.; Hindermann, J.P. FT-IR and TPD Studies on Support-Metal and Promoter-Metal Interaction. Pt and Pd Catalysts. *Catal. Lett.* **1991**, *7*, 359–366. [CrossRef]

40. Pinna, F.; Signoretto, M.; Strukul, G.; Polizzi, S.; Pernicone, N. Pd-SiO$_2$ Catalysts. Stability of β-PdHx as a Function of Pd Dispersion. *React. Kinet. Catal. Lett.* **1997**, *60*, 9–13. [CrossRef]

41. Shesterkina, A.A.; Kirichenko, O.A.; Kozlova, L.M.; Kapustin, G.I.; Mishin, I.V.; Strelkova, A.A.; Kustov, L.M. Liquid-Phase Hydrogenation of Phenylacetylene to Styrene on Silica-Supported Pd–Fe Nanoparticles. *Mendeleev Commun.* **2016**, *26*, 228–230. [CrossRef]

42. Kirichenko, O.; Kapustin, G.; Nissenbaum, V.; Mishin, I.; Kustov, L. Evaluation of Stability of Silica-Supported Fe–Pd and Fe–Pt Nanoparticles in Aerobic Conditions Using Thermal Analysis. *J. Therm. Anal. Calorim.* **2014**, *118*, 749–758. [CrossRef]

43. Kirichenko, O.A.; Strekalova, A.A.; Kapustin, G.I.; Shesterkina, A.A. A New Redox Method for Depositing FeOx on the Surface of Pd(0)/SiO$_2$ Nanoparticles—Catalysts for Selective Phenylacetylene Hydrogenation. *Russ. J. Phys. Chem. A* **2018**, *92*, 2396–2398. [CrossRef]

44. Ouyang, L.; Tian, P.; Da, G.; Xu, X.-C.; Ao, C.; Chen, T.; Si, R.; Xu, J.; Han, Y.-F. The Origin of Active Sites for Direct Synthesis of H_2O_2 on Pd/TiO_2 Catalysts: Interfaces of Pd and PdO Domains. *J. Catal.* **2015**, *321*, 70–80. [CrossRef]

45. Zaki, M.I.; Fouad, N.E.; Bond, G.C.; Tahir, S.F. Temperature-Programmed Reduction of Calcined Chromia-Coated Alumina and Silica Catalysts: Probing Chromium (VI)-Oxygen Species. *Thermochim. Acta* **1996**, *285*, 167–179. [CrossRef]

46. Markov, P.V.; Mashkovsky, I.S.; Bragina, G.O.; Wärnå, J.; Bukhtiyarov, V.I.; Stakheev, A.Y.; Murzin, D.Y. Experimental and Theoretical Analysis of Particle Size Effect in Liquid-Phase Hydrogenation of Diphenylacetylene. *Chem. Eng. J.* **2021**, *404*, 126409. [CrossRef]

47. Jóźwiak, W.K.; Maniecki, T.P. Influence of Atmosphere Kind on Temperature Programmed Decomposition of Noble Metal Chlorides. *Thermochim. Acta* **2005**, *435*, 151–161. [CrossRef]

48. Kachala, V.V.; Khemchyan, L.L.; Kashin, A.S.; Orlov, N.V.; Grachev, A.A.; Zalesskiy, S.S.; Ananikov, V.P. Target-Oriented Analysis of Gaseous, Liquid and Solid Chemical Systems by Mass Spectrometry, Nuclear Magnetic Resonance Spectroscopy and Electron Microscopy. *Russ. Chem. Rev.* **2013**, *82*, 648–685. [CrossRef]

49. Yates, D. The Catalytic Activity of Rhodium in Relation to Its State of Dispersion. *J. Catal.* **1967**, *8*, 348–358. [CrossRef]

50. Kirichenko, O.; Kapustin, G.; Nissenbaum, V.; Strelkova, A.; Shuvalova, E.; Shesterkina, A.; Kustov, L. Thermal Decomposition and Reducibility of Silica-Supported Precursors of Cu, Fe and Cu–Fe Nanoparticles. *J. Therm. Anal. Calorim.* **2018**, *134*, 233–251. [CrossRef]

51. Kirichenko, O.A.; Nissenbaum, V.D.; Kapustin, G.I.; Kustov, L.M. Thermal Analysis of Ammonium Trioxalatometallate Complexes Supported on Titania and Reducibility of Their Decomposition Products. *Thermochim. Acta* **2009**, *494*, 35–39. [CrossRef]

52. Shesterkina, A.A.; Kozlova, L.M.; Kirichenko, O.A.; Kapustin, G.I.; Mishin, I.V.; Kustov, L.M. Influence of the Thermal Treatment Conditions and Composition of Bimetallic Catalysts Fe—Pd/SiO_2 on the Catalytic Properties in Phenylacetylene Hydrogenation. *Russ. Chem. Bull.* **2016**, *65*, 432–439. [CrossRef]